LETTER

https://doi.org/10.1038/s41586-018-0543-y

Clearance of senescent glial cells prevents tau-dependent pathology and cognitive decline

Tyler J. Bussian[1,3], Asef Aziz[2,3], Charlton F. Meyer[2], Barbara L. Swenson[2], Jan M. van Deursen[1,2] & Darren J. Baker[1,2]*

Cellular senescence, which is characterized by an irreversible cell-cycle arrest[1] accompanied by a distinctive secretory phenotype[2], can be induced through various intracellular and extracellular factors. Senescent cells that express the cell cycle inhibitory protein p16^{INK4A} have been found to actively drive naturally occurring age-related tissue deterioration[3,4] and contribute to several diseases associated with ageing, including atherosclerosis[5] and osteoarthritis[6]. Various markers of senescence have been observed in patients with neurodegenerative diseases[7–9]; however, a role for senescent cells in the aetiology of these pathologies is unknown. Here we show a causal link between the accumulation of senescent cells and cognition-associated neuronal loss. We found that the *MAPT^{P301S}PS19* mouse model of tau-dependent neurodegenerative disease[10] accumulates p16^{INK4A}-positive senescent astrocytes and microglia. Clearance of these cells as they arise using *INK-ATTAC* transgenic mice prevents gliosis, hyperphosphorylation of both soluble and insoluble tau leading to neurofibrillary tangle deposition, and degeneration of cortical and hippocampal neurons, thus preserving cognitive function. Pharmacological intervention with a first-generation senolytic modulates tau aggregation. Collectively, these results show that senescent cells have a role in the initiation and progression of tau-mediated disease, and suggest that targeting senescent cells may provide a therapeutic avenue for the treatment of these pathologies.

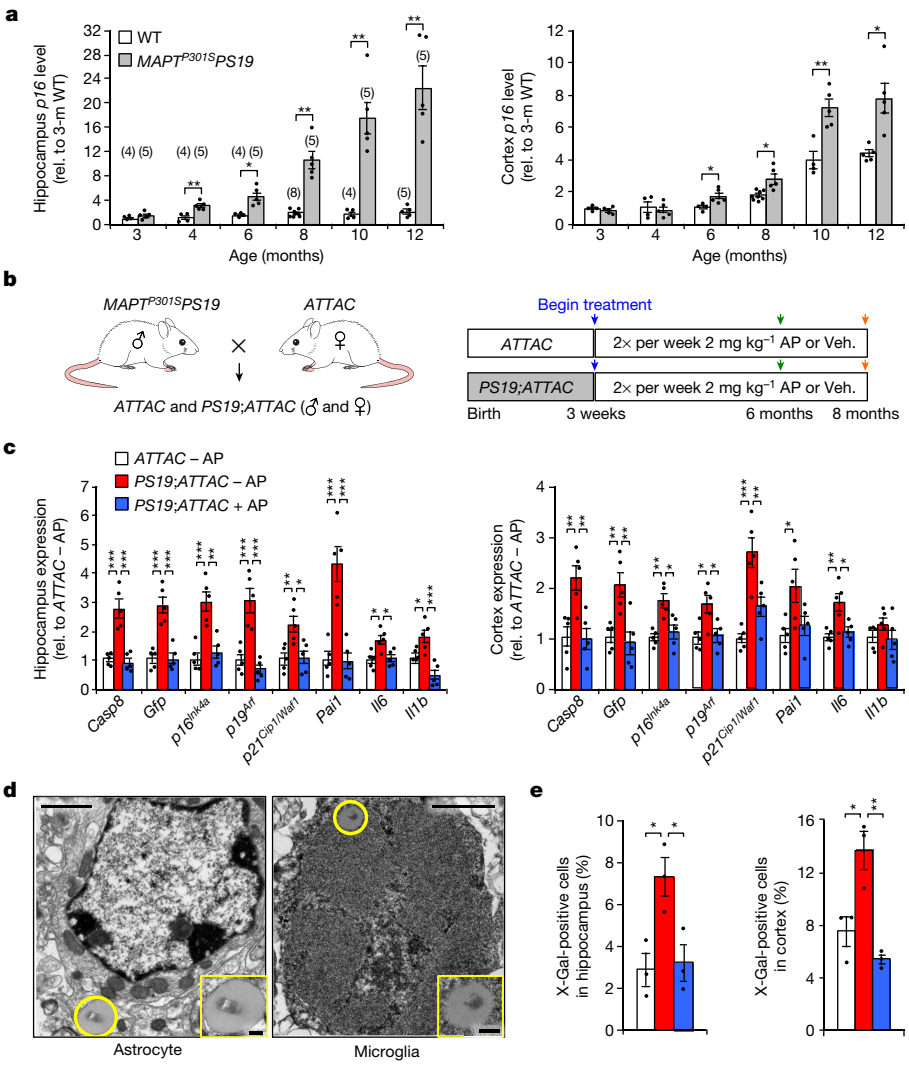

Fig. 1 | Senescent astrocytes and microglia that accumulate in the brains of *MAPT^{P301S}PS19* mice can be removed using the *INK-ATTAC* transgene. a, RT–qPCR analysis of *p16^{Ink4a}* expression in the hippocampus (left) and cortex (right) of wild-type (WT) and *MAPT^{P301S}PS19* mice. The number of mice for each column are indicated in parentheses in the left-hand graph, 2 independent experiments; normalized to the three-month wild-type group. **b**, Study design for the clearance of senescent cells in *PS19*;*ATTAC* mice. Veh., vehicle. **c**, RT–qPCR analysis of the expression of senescence markers in the hippocampus (left) and cortex (cortex) of six-month-old male mice, treated with either vehicle (–AP) or AP20187 (+AP). $n = 5$ mice per group; normalized to the *ATTAC* –AP group. **d**, Electron micrograph showing an X-Gal-positive astrocyte (left) and microglia (right) after SA-β-Gal staining, from a six-month-old vehicle-treated *PS19*;*ATTAC* male mouse. **e**, Quantification of cells containing X-Gal crystals in the hippocampus (left) or the cortex (right) of six-month-old male mice. $n = 3$ male mice per group, 2 independent experiments; the bars are coloured as in **c**. Scale bars, 1 μm (**d**) and 200 nm (**d**, insets). Data are mean ± s.e.m. $^*P < 0.05$; $^{**}P < 0.01$; $^{***}P < 0.001$ (unpaired two-sided *t*-tests with Welch's correction (**a**) and one-way ANOVA with Tukey's multiple comparisons test (**c**, **e**)). Exact *P* values can be found in the accompanying Source Data.

[1]Department of Biochemistry and Molecular Biology, Mayo Clinic, Rochester, MN, USA. [2]Department of Pediatric and Adolescent Medicine, Mayo Clinic, Rochester, MN, USA. [3]These authors contributed equally: Tyler J. Bussian, Asef Aziz. *e-mail: baker.darren@mayo.edu

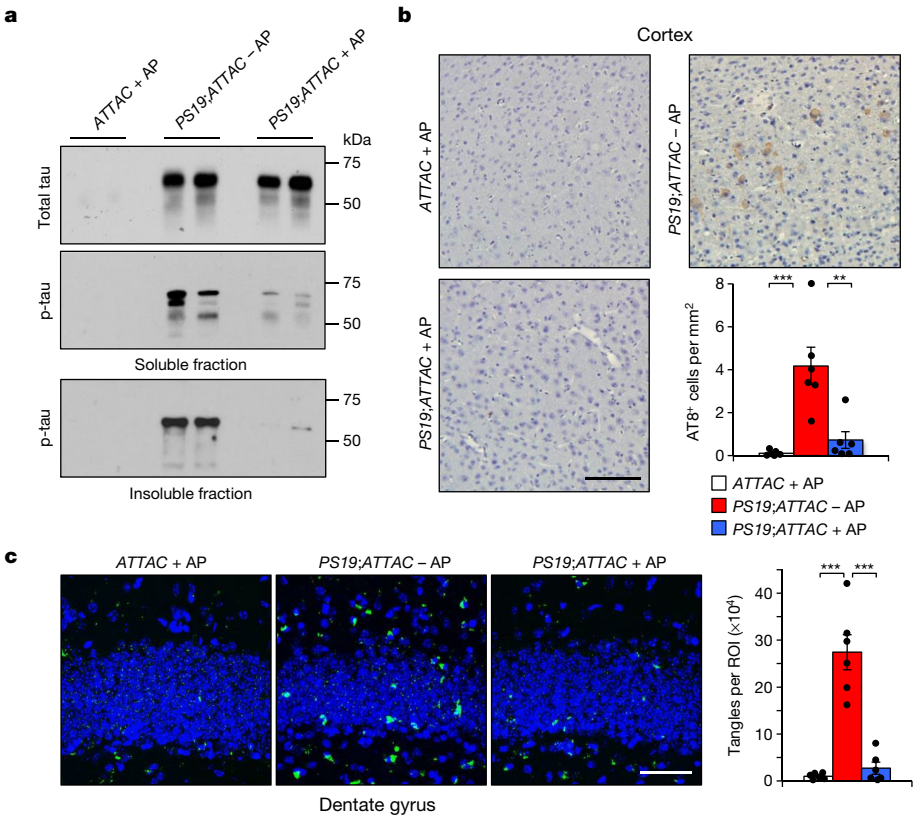

Fig. 2 | Senescent cells promote insoluble tau aggregates. a, Representative western-blot analysis of the whole brain of six-month-old mice for soluble tau (top), soluble phosphorylated tau (S202/T205; middle) and insoluble phosphorylated tau (S202/T205; bottom). ≥3 independent experiments. **b**, Immunostaining and quantification of cortex sections from six-month-old mice for phosphorylated tau (S202/T205) protein aggregates. $n = 6$ mice per group, 3 independent experiments. **c**, Thioflavin-S staining and quantification of neurofibrillary tangles located within the dentate gyrus of eight-month-old mice. $n = 6$ mice per group, 2 independent experiments; normalized to the *ATTAC* + AP group. The bar graph is coloured as in **b**. ROI, region of interest. Scale bars, 100 μm (**b**) and 50 μm (**c**). Data are mean ± s.e.m. $^{**}P < 0.01$; $^{***}P < 0.001$ (one-way ANOVA with Tukey's multiple comparisons test). Exact *P* values can be found in the accompanying Source Data. For gel source data, see Supplementary Fig. 1.

Senescent cells accumulate with ageing and have been shown to contribute to tissue dysfunction[11], although their role in neurodegenerative disease is still unknown. To address this key open question, we selected the transgenic mouse line *MAPT*^{P301S}*PS19* (hereafter *PS19*), which—under the regulation of the mouse prion promoter—expresses high levels of mutant human tau specifically in neurons[10]. The model is characterized by gliosis, neurofibrillary tangle (NFT) deposition, neurodegeneration and loss of cognitive function. Pathology typically initiates in the hippocampus and radiates outwards to the neocortex[10]. First, we performed quantitative PCR with reverse transcription (RT–qPCR) for *p16*^{Ink4a} (also known as *Cdkn2a*) on isolated hippocampi and cortices from wild-type and *PS19* littermates. A significant increase in *p16*^{Ink4a} expression was seen in the *PS19* mice beginning at four months of age in the hippocampus and at six months of age in the cortex (Fig. 1a), which precedes the onset of NFT deposition[10]. Importantly, increased expression of *p16*^{Ink4a} correlated with the expression of widely established senescence markers (Extended Data Fig. 1), indicating that senescent cells accumulate at sites of pathology in the *PS19* model.

To investigate the role of senescent cells in the development of disease, we crossed the *INK-ATTAC* transgene (hereafter *ATTAC*) to the *PS19* strain to eliminate *p16*^{Ink4a}-expressing senescent cells through the twice-weekly administration of AP20187 (hereafter AP)[3,4] from weaning age (Fig. 1b). Hippocampi and cortices isolated from six-month-old vehicle-administered *PS19*;*ATTAC* mice displayed an increased level of the *ATTAC* transgene, as measured by the expression of *Casp8* and *Gfp* (Fig. 1c, Extended Data Fig. 2). Levels of senescence indicators, including the cell-cycle regulators *p16*^{Ink4a}, *p19*^{Arf} (also known as *Cdkn2a*) and *p21*$^{Cip1/Waf1}$ (also known as *Cdkn1a*) and the pro-inflammatory genes *Pai1* (also known as *Serpine1*), *Il6* and *Il1b*, were also increased (Fig. 1c, Extended Data Fig. 2). Administration of AP to *PS19*;*ATTAC* mice maintained the expression of these genes at a level comparable to that of control mice (Fig. 1c, Extended Data Fig. 2). Importantly, treatment of *ATTAC* mice that lacked the *PS19* transgene with AP had no effect on the expression of these markers (Extended Data Fig. 2). Thus, AP administration effectively and selectively cleared senescent cells in the hippocampus and cortex of *PS19*;*ATTAC* mice.

To understand the mechanistic contribution of senescence to tau-mediated pathology, we sought to identify the specific cell types that were becoming senescent. First, we stained cortices and hippocampi from six-month-old vehicle-treated *ATTAC* and *PS19*;*ATTAC* mice and AP-treated *PS19*;*ATTAC* mice for senescence-associated-β-galactosidase (SA-β-Gal)[12] and screened for cells that contained 5-bromo-4-chloro-3-indolyl-β-D-galactopyranoside (X-Gal) crystals by transmission electron microscopy[13]. We found that cells that clearly and morphologically resembled astrocytes or microglia contained X-Gal crystals, irrespective of the treatment group from which they arose (Fig. 1d). By contrast, no crystals were found in any clearly identifiable neurons (Extended Data Fig. 3). Compared with control mice, vehicle-treated *PS19*;*ATTAC* mice had nearly double the number of cells containing X-Gal crystals in both the hippocampus and the cortex (Fig. 1e), whereas AP-treated *PS19*;*ATTAC* mice had a similar incidence of X-Gal crystals as control mice (Fig. 1e). To validate that senescence was affecting astrocytes and microglia, we performed fluorescence-activated cell sorting (FACS) on six-month-old wild-type and *PS19* mice (Extended Data Fig. 4a). Isolated astrocytes and microglia had increased expression of senescence-associated genes, including *p16*^{Ink4a} (Extended Data Fig. 4b, c). A similar induction was not observed in oligodendrocytes or neuron-enriched CD56^{+} cells (Extended Data Figs. 4d, e, 5), supporting the conclusion that senescence occurs primarily in astrocytes and microglia of *PS19* mice.

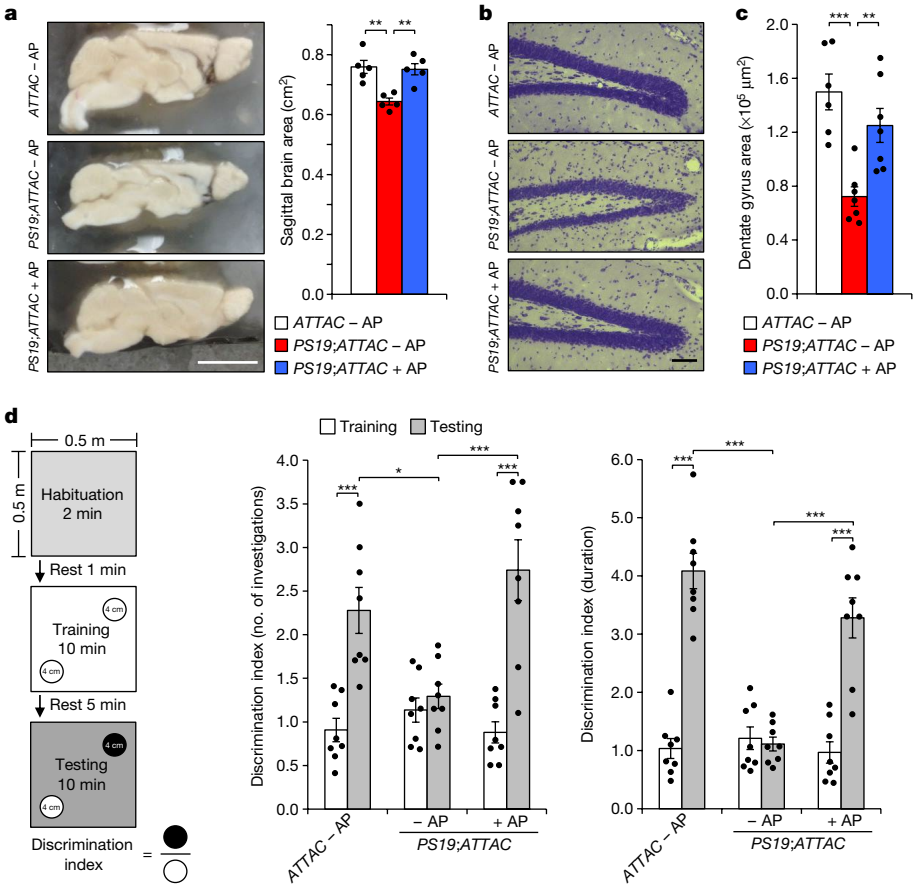

Fig. 3 | Senescent cells drive neurodegenerative disease. a, Sagittal midline brain area images (left) and quantification (right) of eight-month-old mice. $n = 5$ males per group, 2 independent experiments. **b**, Nissl stains of the dentate gyrus (left) and quantification (right) from eight-month-old mice. **c**, Average area of the dentate gyrus (measuring the pyramidal neuron layer) from serial, coronal NeuN-stained free-floating sections. $n = 6$ *ATTAC* –AP and $n = 7$ *PS19*;*ATTAC* – AP and *PS19*;*ATTAC* + AP mice, 2 independent experiments. **d**, Setup of the novel-object recognition experiment (left) and average ratio for the number of investigations (middle) and duration of those investigations (right). $n = 8$ female mice per group. Scale bars, 0.5 cm (**a**) and 100 µm (**b**). Data are mean ± s.e.m. $^*P < 0.05$; $^{**}P < 0.01$; $^{***}P < 0.001$ (one-way ANOVA with Tukey's multiple comparisons test (**a**, **c**) and two-way ANOVA with Tukey's multiple comparisons test (**d**)). Exact *P* values can be found in the accompanying Source Data.

To verify that the administration of AP selectively targeted senescent cells, we prepared in vitro cultures of primary microglia and astrocytes isolated from *ATTAC* mice. These cultures were not sensitive to AP-mediated elimination in the absence of senescence-inducing stimuli (Extended Data Fig. 6). Furthermore, for *ATTAC* transgenic mice in vivo, the short-term administration of AP did not promote excessive cellular death (Extended Data Fig. 7a), and extended treatment with AP did not result in increased proliferation of microglia (Extended Data Fig. 7b).

PS19 mice present progressive gliosis with disease progression[10]. To assess whether the administration of AP affected this process, RT–qPCR was performed on the hippocampi of six-month-old mice for markers of astrocytes (*Gfap* and *S100b*) and microglia (*Cd11b*, also known as *Itgam*). Vehicle-treated *PS19*;*ATTAC* mice had an approximately two- to threefold induction in these markers, whereas AP-treated *PS19*;*ATTAC* mice expressed these markers at a similar level to control mice (Extended Data Fig. 8a, b). Immunohistochemistry staining for GFAP and IBA1 confirmed these observations (Extended Data Fig. 8c, d). Taken together, these results suggest that both senescent glial cells and gliosis are eliminated upon the administration of AP in *PS19*;*ATTAC* mice.

A distinguishing characteristic of *PS19* mice is the development of aggregates consisting of hyperphosphorylated tau protein by six months of age[10]. To assess whether tau aggregation was affected by senescence clearance, we measured the levels of soluble total and phosphorylated tau (S202/T205) in addition to the level of insoluble phosphorylated tau in vehicle-treated *PS19*;*ATTAC* and AP-treated *ATTAC* and *PS19*;*ATTAC* mice. As expected[10], vehicle-treated *PS19*;*ATTAC* mice displayed increased levels both of soluble total and phosphorylated tau and of insoluble phosphorylated tau (Fig. 2a, Extended Data Fig. 9a, b). AP-treated *PS19*;*ATTAC* mice had identical levels of soluble total tau to vehicle-treated *PS19*;*ATTAC* mice (Fig. 2a), indicating that overexpression of tau from the transgene was maintained. Treatment of *PS19*;*ATTAC* mice with AP significantly reduced the amount of phosphorylated tau in both the soluble and the insoluble fractions (Fig. 2a, Extended Data Fig. 9b). Immunohistochemistry staining for phospho-tau modifications at S202/T205, T231 and S396 confirmed that the clearance of senescent cells attenuated tau phosphorylation at several residues that are relevant for tau aggregation (Fig. 2b, Extended Data Fig. 9c). Additionally, the staining of brain sections of eight-month-old mice from these same groups with thioflavin-S revealed that NFT deposition in the dentate gyrus—the site of neurogenesis in the hippocampus that is traditionally associated with memory formation and cognition[14]—was substantially reduced when senescent cells were removed (Fig. 2c). Collectively, these results indicate that the accumulation of senescent cells promotes the formation of hyperphosphorylated tau aggregates.

PS19 mice show neurodegeneration by eight months of age[10]. As NFT deposition was attenuated upon treatment with AP in both the cortex and the hippocampus of *PS19*;*ATTAC* mice, we performed assessments for degeneration in these areas. The overt brain size of vehicle-treated *PS19*;*ATTAC* mice was reduced compared to both

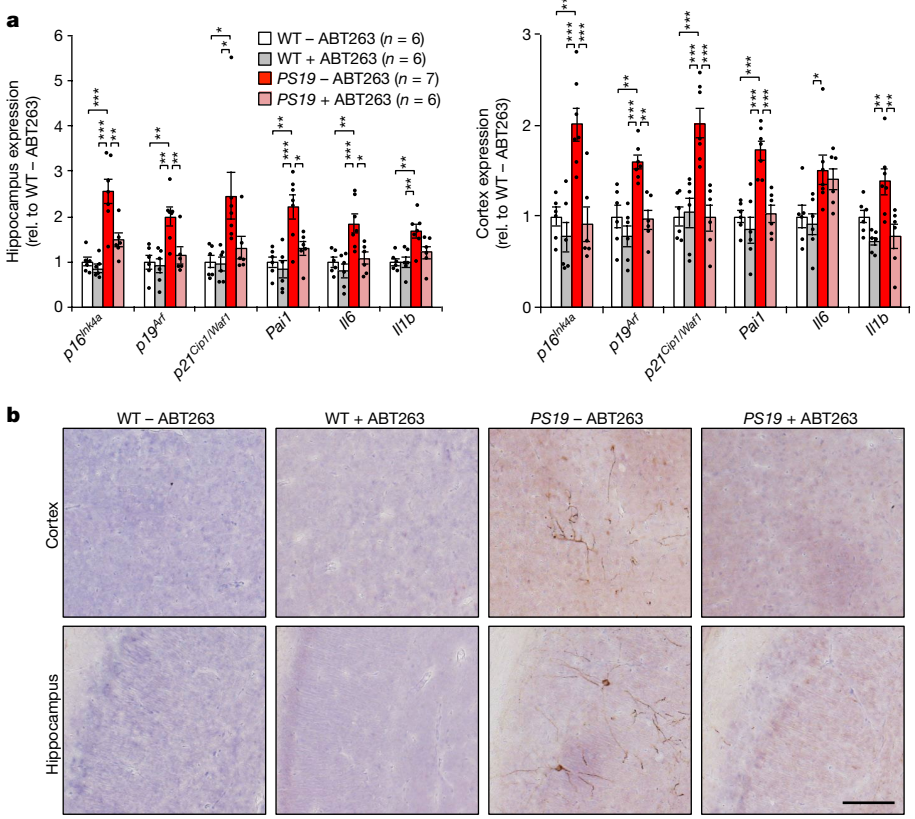

Fig. 4 | ABT263 can modulate senescent cells and attenuate tau phosphorylation. a, RT–qPCR analysis of the expression of senescence markers from the hippocampus (left) and the cortex (right) of six-month-old mice treated with either vehicle (–ABT263) or ABT263 (+ABT263). Number of mice is as indicated; normalized to the WT – ABT263 group. **b**, Representative immunostaining of cortex (top) and hippocampal (bottom) sections for phosphorylated tau (S202/T205) protein aggregates. $n = 4$ mice per group, 2 independent experiments. Scale bar, 100 μm. Data are mean ± s.e.m. $^{*}P < 0.05$; $^{**}P < 0.01$; $^{***}P < 0.001$ (one-way ANOVA with Tukey's multiple comparisons test). Exact *P* values can be found in the accompanying Source Data.

ATTAC and AP-treated *PS19*;*ATTAC* mice (Fig. 3a). In addition, we observed localized neurodegeneration in the dentate gyrus of the hippocampus through Nissl staining in vehicle-treated *PS19*;*ATTAC* mice (Fig. 3b). The administration of AP prevented thinning of the dentate gyrus and increased neuron density. Sequential coronal sectioning and NeuN staining revealed that the dentate gyrus was significantly reduced in area in vehicle-treated *PS19*;*ATTAC* mice (Fig. 3c), further demonstrating that senescent cells promote neurodegeneration in *PS19* mice.

To test whether the effects observed upon administration of AP resulted in improved cognitive function, we performed novel-scent discrimination assessments to test for changes in short-term memory[15] (for experimental setup, see Fig. 3d). Whereas AP-treated *ATTAC* mice were more inquisitive towards the novel scent during the testing phase, vehicle-treated *PS19*;*ATTAC* mice were not (Fig. 3d). By contrast, AP-treated *PS19*;*ATTAC* mice behaved nearly identically to control (AP-treated *ATTAC*) mice, indicating that the elimination of senescent cells mitigated the short-term memory loss observed in vehicle-treated *PS19*;*ATTAC* mice. Notably, the overall distance travelled by mice in all groups was unchanged (data not shown), and similar results were obtained in novel-object discrimination tests that had the same setup but used visual cues instead of scents (Extended Data Fig. 10). Thus, these results demonstrate that senescent cells drive neurodegeneration and loss of cognition in *PS19* mice.

Last, we tested whether the pharmacological elimination of senescent cells with the senolytic ABT263 (navitoclax)[5,6,16,17] resulted in similar effects to our genetic interventions in *PS19* mice. Recent work has demonstrated a therapeutic effect in orthotopically implanted glioblastomas of the peripheral administration of ABT263[18]. Wild-type and *PS19* mice were treated with a repeating schedule of ABT263, beginning at weaning age and continuing until the mice reached six months of age. Notably, this treatment prevented the upregulation of senescence-associated genes (Fig. 4a) and attenuated tau phosphorylation in *PS19* mice (Fig. 4b), indicating that senolytic interventions can recapitulate key observations from transgenic mouse models of senescent-cell ablation.

The mechanistic contribution of cells with features reminiscent of senescence to the pathophysiology of neurodegenerative diseases has been a common question in recent years[7–9,19–21]. Furthermore, recent work has suggested that senescent cells may contribute to the pathology of Parkinson's disease in both mice and humans[22]. Here we show that the continuous clearance of $p16^{Ink4a}$-expressing senescent cells before disease onset in a model of aggressive tauopathy has a marked effect on various aspects of disease progression, including gliosis, NFT formation, neurodegeneration and cognitive decline. Senescent-cell clearance also has a notable effect on the accumulation of phosphorylated tau protein in both the soluble and insoluble fractions. The amount of total soluble tau was unchanged in AP-treated *PS19*;*ATTAC* mice (Fig. 2a), indicating that the aberrant hyperphosphorylation of tau protein and subsequent aggregation into NFTs is mediated by extracellular signalling from $p16^{Ink4a}$-expressing senescent glial cells. The molecular mechanisms that senescent astrocytes and microglia exploit to promote the pathological conversion of tau into NFTs within neurons require additional investigation. The absence of neurodegeneration in mice treated with AP (Fig. 3) demonstrates that the attenuation of disease severity does not result from the clearance of neurons containing NFTs. However, it is important to leave open the possibility that other models of neurodegenerative disease may exhibit senescence-associated alterations in cell types other than those observed in the present study. Regardless, based on our observations, it is likely that intervening with senescent-cell accumulation in these models would also reduce the

severity of disease. As this study was designed to prevent senescent cells from accumulating to determine how this affects disease, future studies of senolysis in established disease models will be necessary to determine whether senolytic strategies could translate into the clinic to halt or perhaps revert disease. As senescent cells exhibit a unique and identifiable senescence-associated secretory phenotype, exploiting this phenotype may serve as a possible therapeutic avenue to attenuate many tau-dependent pathologies. Our observation that *p16*^{Ink4a} expression increases before the onset of NFT aggregation further supports the now commonly held belief that early intervention in these diseases is essential to provide more beneficial effects for patients.

Online content

Any methods, additional references, Nature Research reporting summaries, source data, statements of data availability and associated accession codes are available at https://doi.org/10.1038/s41586-018-0543-y.

Received: 3 November 2017; Accepted: 29 August 2018;
Published online 19 September 2018.

1. Hayflick, L. & Moorhead, P. S. The serial cultivation of human diploid cell strains. *Exp. Cell Res.* **25**, 585–621 (1961).
2. Coppé, J. P. et al. Senescence-associated secretory phenotypes reveal cell-nonautonomous functions of oncogenic RAS and the p53 tumor suppressor. *PLoS Biol.* **6**, e301 (2008).
3. Baker, D. J. et al. Naturally occurring p16^{Ink4a}-positive cells shorten healthy lifespan. *Nature* **530**, 184–189 (2016).
4. Baker, D. J. et al. Clearance of p16^{Ink4a}-positive senescent cells delays ageing-associated disorders. *Nature* **479**, 232–236 (2011).
5. Childs, B. G. et al. Senescent intimal foam cells are deleterious at all stages of atherosclerosis. *Science* **354**, 472–477 (2016).
6. Jeon, O. H. et al. Local clearance of senescent cells attenuates the development of post-traumatic osteoarthritis and creates a pro-regenerative environment. *Nat. Med.* **23**, 775–781 (2017).
7. Bhat, R. et al. Astrocyte senescence as a component of Alzheimer's disease. *PLoS ONE* **7**, e45069 (2012).
8. Tan, F. C., Hutchison, E. R., Eitan, E. & Mattson, M. P. Are there roles for brain cell senescence in aging and neurodegenerative disorders? *Biogerontology* **15**, 643–660 (2014).
9. Luo, X. G., Ding, J. Q. & Chen, S. D. Microglia in the aging brain: relevance to neurodegeneration. *Mol. Neurodegener.* **5**, 12 (2010).
10. Yoshiyama, Y. et al. Synapse loss and microglial activation precede tangles in a P301S tauopathy mouse model. *Neuron* **53**, 337–351 (2007).
11. Childs, B. G. et al. Senescent cells: an emerging target for diseases of ageing. *Nat. Rev. Drug Discov.* **16**, 718–735 (2017).
12. Dimri, G. P. et al. A biomarker that identifies senescent human cells in culture and in aging skin *in vivo*. *Proc. Natl Acad. Sci. USA* **92**, 9363–9367 (1995).
13. Stollewerk, A., Klämbt, C. & Cantera, R. Electron microscopic analysis of *Drosophila* midline glia during embryogenesis and larval development using beta-galactosidase expression as endogenous cell marker. *Microsc. Res. Tech.* **35**, 294–306 (1996).
14. Ming, G. L. & Song, H. Adult neurogenesis in the mammalian brain: significant answers and significant questions. *Neuron* **70**, 687–702 (2011).
15. Buenz, E. J. et al. Apoptosis of hippocampal pyramidal neurons is virus independent in a mouse model of acute neurovirulent picornavirus infection. *Am. J. Pathol.* **175**, 668–684 (2009).
16. Chang, J. et al. Clearance of senescent cells by ABT263 rejuvenates aged hematopoietic stem cells in mice. *Nat. Med.* **22**, 78–83 (2016).
17. Zhu, Y. et al. Identification of a novel senolytic agent, navitoclax, targeting the Bcl-2 family of anti-apoptotic factors. *Aging Cell* **15**, 428–435 (2016).
18. Karpel-Massler, G. et al. Induction of synthetic lethality in IDH1-mutated gliomas through inhibition of Bcl-xL. *Nat. Commun.* **8**, 1067 (2017).
19. Flanary, B. E., Sammons, N. W., Nguyen, C., Walker, D. & Streit, W. J. Evidence that aging and amyloid promote microglial cell senescence. *Rejuvenation Res.* **10**, 61–74 (2007).
20. Salminen, A. et al. Astrocytes in the aging brain express characteristics of senescence-associated secretory phenotype. *Eur. J. Neurosci.* **34**, 3–11 (2011).
21. Streit, W. J., Braak, H., Xue, Q. S. & Bechmann, I. Dystrophic (senescent) rather than activated microglial cells are associated with tau pathology and likely precede neurodegeneration in Alzheimer's disease. *Acta Neuropathol.* **118**, 475–485 (2009).
22. Chinta, S. J. et al. Cellular senescence is induced by the environmental neurotoxin paraquat and contributes to neuropathology linked to Parkinson's disease. *Cell Rep.* **22**, 930–940 (2018).

Acknowledgements The authors thank C. H. Cho for numerous contributions to the experiments; the laboratory of C. Howe and specifically M. Standiford for help with the microglia and astrocyte cultures; M. Poeschla for assistance with the phospho-tau immunohistochemistry; G. Nelson for genotyping and animal support; B. Childs for input and assistance in Gal-TEM; the Mayo Clinic Microscopy and Cell Analysis Core and staff for assistance with flow cytometry and transmission electron microscopy; the Mayo Clinic Medical Genome Facility Gene Expression Core for RT–qPCR instrumentation; and R. Petersen and C. Howe for feedback on the manuscript. This work was supported by the Ellison Medical Foundation, the Glenn Foundation for Medical Research, the National Institutes of Health (R01AG053229), the Mayo Clinic Children's Research Center and the Alzheimer's Disease Research Center of Mayo Clinic (all to D.J.B.).

Reviewer information *Nature* thanks M. Serrano and the other anonymous reviewer(s) for their contribution to the peer review of this work.

Author contributions T.J.B. and A.A. performed most of the experiments. C.F.M. assisted with the senescent cell identification by Gal-TEM and FACS. B.L.S. performed immunohistochemistry assessments. J.M.v.D. assisted with experimental design and data interpretation. The manuscript was written by T.J.B. and D.J.B. All authors discussed results, made figures and edited the manuscript. D.J.B. conceived, directed and supervised all aspects of the study.

Competing interests D.J.B. and J.M.v.D. are co-inventors on patent applications licensed to or filed by Unity Biotechnology, a company developing senolytic medicines, including small molecules that selectively eliminate senescent cells. J.M.v.D. is a co-founder of Unity Biotechnology. Research in the Baker laboratory has been reviewed by the Mayo Clinic Conflict of Interest Review Board and is being conducted in compliance with Mayo Clinic Conflict of Interest policies.

Additional information
Extended data is available for this paper at https://doi.org/10.1038/s41586-018-0543-y.
Supplementary information is available for this paper at https://doi.org/10.1038/s41586-018-0543-y.
Reprints and permissions information is available at http://www.nature.com/reprints.
Correspondence and requests for materials should be addressed to D.J.B.
Publisher's note: Springer Nature remains neutral with regard to jurisdictional claims in published maps and institutional affiliations.

METHODS

Mouse strains and drug treatment. *MAPT*^{P301S}*PS19* (*PS19*) mice were purchased from The Jackson Laboratory (stock no. 008169) and bred to C57BL/6 for three generations. C57BL/6 *ATTAC* transgenic mice are as previously described[3,4]. Male *PS19* mice were bred to *ATTAC* females to generate cohorts of *ATTAC* and *PS19*;*ATTAC* mice. All mice were on a pure C57BL/6 genetic background. Mice from this cohort were randomly assigned to receive AP20187 (AP; B/B homodimerizer; Clontech) or vehicle twice a week beginning at weaning age (3 weeks). Dosing of AP was 2.0 mg per kg body weight. Six-month-old short-term AP-pulse-treated mice (Extended Data Fig. 6a) received a dose of 10 mg per kg body weight for five consecutive days before tissue collection. Senolytic intervention was performed in C57BL/6 wild-type and *PS19* mice. At weaning, mice were assigned to receive either ABT263 (Cayman, 923564-51-6) or vehicle (Phosal 50 PG, Lipoid NC0130871, 60%; PEG400, Sigma 91893, 30%; ethanol, 10%). ABT263 was administered by oral gavage at a dose of 50 mg per kg body weight on a repeating regimen of five consecutive days of treatment followed by 16 days of rest. Mice were housed in a 12 h:12 h light:dark cycle environment in pathogen-free barrier conditions as previously described in detail[3]. Compliance with relevant ethical regulations and all animal procedures were reviewed and approved by the Mayo Clinic Institutional Animal Care and Use Committee.

Statistical analysis. Prism software was used for all statistical analysis. A Student's two-tailed unpaired *t*-test with Welch's correction was used in Fig. 1a and Extended Data Fig. 4b–e; two-way ANOVA with Tukey's multiple comparisons test was used for Fig. 3d and Extended Data Fig. 10; and one-way ANOVA with Tukey's multiple comparisons test was used in all other figures. For consistency in these comparisons, the following denotes significance in all figures: $*P < 0.05$, $**P < 0.01$, $***P < 0.001$. We note that no power calculations were used. Sample sizes are based on previously published experiments in which differences were observed. No samples were excluded. Investigators were blinded to allocation during experiments and outcome assessment, except for rare instances in which blinding was not possible.

Senescence-associated β-galactosidase transmission electron microscopy (Gal-TEM). Detection of X-Gal crystals by TEM after senescence-associated β-galactosidase (SA-β-Gal) staining was performed as previously described[3,5], with the following alterations to accommodate central nervous tissue. Mice were transcardially perfused with ice-cold Dulbecco's phosphate-buffered saline (DPBS; pH 7.4) until fluid run-off was clear. This was followed by perfusion with 4% paraformaldehyde (PFA) for 10 min at a rate of 3 ml min^{-1}, and then ice-cold DPBS was perfused again for 2 min at the same rate to remove the remaining fixative. Brains were then isolated and the hippocampus and cortex were dissected out. A 1 mm × 1 mm piece from the CA1 and M1 regions, respectively, was then incubated in SA-β-Gal staining solution (Cell Signaling) at 37 °C for 6 h (hippocampus) or 18 h (cortex). The samples were placed in Trump's fixative overnight at 4 °C before being processed for routine transmission electron microscopy (dehydration by xylene-alcohol series, osmium tetroxide staining, and Epon resin embedding). Images were acquired and quantified using a Jeol 1400+ electron microscope with an 80-kV acceleration voltage. Two grids from each tissue were produced, and >100 cells were scanned per grid at a magnification of 20,000× to detect cells containing X-Gal crystals. On average, half of all cells examined were neurons. Cells with one or more crystals, and the total number of cells, were counted. Cells containing crystals were imaged and independently assessed for distinguishing morphology. To define cell type, the following criteria were applied. Astrocytes: circular nucleus with spattered electron density pattern; microglia: abnormally shaped nucleus with a much darker, often phagosome-containing cytoplasm; and neuron: large circular nucleus with less electron density and periodically denoted by an offshooting axon. Only cells with morphology consistent with astrocytes or microglia were clearly positive for X-gal crystals.

Western blotting for soluble and sarkosyl insoluble proteins. Half brains were weighed and homogenized in 5× volume of Buffer I (50 mM Tris base (pH 7.4), 50 mM NaCl, 1 mM EDTA, 1 mM phenylmethylsulfonyl fluoride (PMSF), 1× Halt Protease and Phosphatase Inhibitor Cocktail (Thermo)). Two hundred and fifty microlitres of the homogenate was then added to an equal volume of Buffer S (50 mM Tris (pH 8.0), 274 mM NaCl, 5 mM KCl, 1 mM PMSF, 1X Halt Protease and Phosphatase Inhibitor Cocktail (Thermo)) and ultracentrifuged at 150,000*g* for 15 min at 4 °C. The supernatant (S1-soluble protein fraction) was transferred to a new tube and the pellet homogenized in 3× volume of sucrose buffer (10 mM Tris (pH 7.4), 0.8M NaCl, 10% sucrose, 1 mM EGTA, 1 mM PMSF) before being ultracentrifuged at 150,000*g* for 15 min at 4 °C. The pellet was discarded and the supernatant incubated with sarkosyl (sodium lauroyl sarcosinate) at a final concentration of 1% for 1 h at 37 °C. After incubation, the samples were ultracentrifuged at 150,000g for 30 min at 4 °C. The supernatant was discarded and the pellet was resuspended in 25 µl Buffer F (10 mM Tris (pH 8.0), 1 mM EDTA) to obtain the insoluble protein fraction (S2). Equal parts of 2× laemmli buffer (Bio-Rad) containing 5% β-mercaptoethanol was added to each fraction (S1 and S2) and boiled at 100 °C for 15 min to prepare the sarkosyl-soluble and -insoluble protein lysates. For total protein lysate, 90 µl of the homogenate (half brain in 5X volume Buffer I) was added to 110 µl of Buffer T (2% SDS, 50 mM Tris (pH 7.4), 274 mM NaCl, 5 mM KCl, 5 mM EDTA, 1% Triton-X-100, 1 mM PMSF, X Halt Protease and Phosphatase Inhibitor Cocktail (Thermo)). The samples were then sonicated and centrifuged at 16,000*g* for 15 min at 4 °C to remove debris. The supernatant was removed and added to equal parts 2× laemmli buffer with 5% β-mercaptoethanol and boiled at 100 °C for 15 min to prepare the total protein lysate. Western blotting was performed as previously described[23]. Blots were probed with antibodies for total tau (Thermo Fisher; MN1000, 1:5,000) and phospho-tau S202/T205 (Thermo Fisher; MN1020, 1:1,000). Ponceau-S staining was performed to normalize lysate loading for the total- and S1-fraction lysates. Quantification was performed using ImageJ as previously described[3].

Quantitative RT–PCR. RNA extraction, cDNA synthesis and RT–qPCR analysis were performed on hippocampi and cortical samples from mouse brains as previously described[24]. Primers used to amplify *Casp8*, *GFP*, *p16*^{Ink4a}, *p19*^{Arf}, *p21*, *Pai1*, *Il-6*, *Il-1b* and *Cd11b* were as previously described[3,5,24]. The following additional primers were used: *Gfap* forward 5′-CCTTCTGACACGGATTTGGT-3′, reverse 5′-TAAGCTAGCCCTGGACATCG-3′; *S100b* forward 5′-CCGGAGTACTGG TGGAAGAC-3′, reverse 5′-GGACACTGAAGCCAGAGAGG-3′; *Aqp4* forward 5′-TGAGCTCCACATCAGGACAG-3′, reverse 5′-TCCAGCTCGATCTT TTGGAC-3′; *Cx3cr1* forward 5′-GTTCCAAAGGCCACAATGTC-3′, reverse 5′-TGAGTGACTGGCACTTCCTG-3′; *Olig2* forward 5′-CCCCA GGGATGATCTAAGC-3′, reverse 5′-CAGAGCCAGGTTCTCCTCC-3′; *Nefl* forward 5′-AGGCCATCTTGACATTGAGG-3′, reverse 5′-GCAGAATGCAGAC ATTAGCG-3′; *Tbp* forward 5′-GGCCTCTCAGAAGCATCACTA-3′, reverse 5′-GCCAAGCCCTGAGCATAA-3′. Expression for all experiments was normalized first to *Tbp*.

Immunohistochemistry and immunofluorescence staining. Mice were transcardially perfused as described in 'Senescence-associated β-galactosidase transmission electron microscopy (Gal-TEM)'. Brains were stored in 4% PFA overnight at 4 °C and then cryoprotected by incubating in a 30% sucrose solution for 48 h at 4 °C. Samples were sectioned into 30-µM-thick coronal sections and stored in antifreeze solution (300 g sucrose, 300 ml ethylene glycol, 500 ml PBS) at −20 °C. Nissl staining (bregma −2.1 to −2.4 mm), thioflavin S staining (bregma −1.4 to −1.6 mm), and phospho-tau S202/S205 (Thermo Fisher, MN1020; 1:500), phospho-tau T231 (Thermo Fisher, MN1040; 1:500), phospho-tau S396 (Abcam, 109390; 1:500), and GFAP (Dako, Z0334; 1:500) and IBA1 (Novus, NB100-1028; 1:100) immunohistochemistry staining (bregma 1.6 to 1.0 mm and lateral 2.0 to 2.7 mm) was performed on free-floating sections as described[25–27]. NeuN staining (EMD, MAB377; 1:200) of five sections (between bregma −1.3 to −2.5) to measure the dentate gyrus area was performed as previously described[28]. For cellular proliferation assays, mice were injected with EdU (Carbosynth, NE08701; 75 mg kg^{-1}) intraperitoneally 24 h before euthanasia. Imaging of EdU-positive cells (lateral 0.75 to 1.25 mm) was performed following the manufacturer's instructions (Invitrogen Click-iT EdU Alexa Fluor 488 Imaging Kit, C10337). IBA1 (Wako, 019-19741; 1:500) immunofluorescent staining and IBA1/EdU colocalization assessments were performed as previously described[28]. TUNEL staining (lateral 0.75 to 1.25 mm) was performed according to the manufacturer's instructions (Roche In situ Cell Death Detection Kit, Fluorescein: 11684795910). Thioflavin S, EdU/IBA1 colocalization, and in vivo TUNEL-stained images were acquired on a Zeiss LSM 780 confocal system using multi-track configuration.

Single-cell preparation and FACS. Dissociation of cerebral tissue was performed using the Adult Brain Dissociation kit from Miltenyi (MACS, 130-107-677), according to the manufacturer's instructions. Samples were then incubated with a viability dye, LIVE/DEAD Aqua (Invitrogen, L34966; 1:250) followed by incubation with CD11b eFluor 450 (eBioscience, 48-0112-80, 1:100), CD45 APC eFluor 780 (eBioscience, 47-0451-82; 1:200), Glast1 PE (Miltenyi Biotec, 130-095-821; 1:100), O1 AF 700 (R&D Systems, FAB1327N-100UG; 1:100) and CD56 APC (R&D Systems, FAB7820A; 1:100). These samples were then sorted using a FACSAria IIu SORP (BD Biosciences), with gating parameters created using FACSDiva 8.0.1 (BD Biosciences). A precise gating strategy was used to maximize the purification of each isolated cell population. In brief, populations were isolated first by a negative report of the viability dye indicating the cell is viable (Extended Data Fig. 4), followed by a positive report of the desired marker, then negative reports of the other labels used. This strategy allowed for live cells containing only the desired marker to be sorted, while eliminating dead cells. Cells were sorted directly into lysis buffer and RNA was extracted with RNeasy Micro kits according to the manufacturer's instructions (Qiagen, cat no. 74004). cDNA synthesis and RT–qPCR analysis were performed as described above.

Novel-object recognition. Novel-object recognition testing was performed as previously described[15]. In brief, mice from each cohort were acclimatized to a 50 cm × 50 cm testing environment for a period of two minutes. After acclimatization, the mice were removed, the testing area was cleaned with 70% ethanol, and two

identical scented candles were placed in either corner of the testing area approximately 5 cm from either wall. Mice were reintroduced, and the ratio of both the number of visits and the time spent at each candle was recorded for a period of ten minutes. Recording was performed from above (Panasonic WV-CP294) and all video files were analysed with TopScan Version 3.00 (Clever Sys). Afterwards, the mice were removed, the testing area cleaned with 70% ethanol, and one candle was replaced with a novel scent. The mice were reintroduced and the number of visits and total time per candle was recorded as before. Testing was also performed with visual stimuli, by placing identical toy brick towers at either corner and then replacing with a different toy brick tower in the testing phase, using the same experimental paradigm monitoring for the number of investigations.

In vitro astrocyte and microglia culture. Astrocyte and microglia primary cultures were prepared in tandem from mixed glial cultures as previously described[29]. C57BL/6 wild-type and *ATTAC* pups (postnatal day (P)0–P3) were euthanized, and the cerebellum was discarded. Meninges were removed from the remaning tissue using forceps and a dissection scope. Cleaned cerebral tissue was placed in chilled Earle's Balanced Salt Solution with HEPES (EBSH) (NaCl 120 mM, NaH_2PO_4 10 mM, KCl 2.5 mM, $C_6H_{12}O_6$ 20 mM, HEPES 20 mM, $NaHCO_3$ 10 mM, BSA 0.3%, H_2O) until the remaining mice were euthanized, and then mice were pooled together on the basis of genotype (3–4 brains per group). The tissue was minced using a razor blade and dissociated by shaking in a 0.025% Trypsin/EBSH solution at 37 °C for 30 min. FBS and $MgSO_4$ (3.82%)/ DNase I (1 mg ml^{-1}) were added, and the sample was placed on ice for 5 min to halt trypsinization. Samples were mixed and centrifuged at 200*g* at 25 °C for 5 min. The supernatant was discarded, and the remaining pellet was resuspended in EBSH. Tissue was triturated using a 1 ml pipette to completely dissociate the sample and allowed to settle for 5 min to remove large debris. Samples were then transferred to clean tubes and underlaid with a 4% BSA/EBSH solution. The tissue was then centrifuged at 100*g* at 25 °C for 8 min. Cells were counted using trypan blue and a haemocytometer and plated on a poly-D-lysine-coated T75 dish (7–10 million cells per flask) with glial cell culture medium (GCM) consisting of DMEM with 10% FBS, sodium pyruvate (1 mM), Pen/Strep (500 μg ml^{-1}), and InvivoGen Primocin (100 μg ml^{-1}). Cultures were grown for 14 days (37 °C, ambient O_2) with medium changes every 4 days. Microglia were isolated as previously described[30] using the EasySep Mouse CD11b Positive Selection Kit from Stem Cell (cat. no. 18970). Microglia were collected and plated on 10-well glass slides (5,000 cells per well) and cultured for 6 days in GCM with LADMAC-conditioned medium (20%, provided by the Howe laboratory) before further experimentation. This conditioned medium aids in the proliferation and maintenance of microglia cultures through the secretion of macrophage colony-stimulating factor by the LADMAC cells[31]. Microglia were allowed to proliferate for 6 days before experimentation. The mixed glial culture flow-through from the EasySep CD11b kit was replated in GCM on a poly-D-lysine-coated T75 dish (10 million cells per flask). These cultures then underwent purification for astrocytes as previously described[29]. After 48 h, flasks were placed on an orbital shaker and agitated at 200 r.p.m. for two 24-h periods with medium refreshed once during and after the shaking. Flasks were then exposed to GCM containing liposomal clodronate (Clodrosome, 8909; 100 μg ml^{-1}) for 72 h to remove any remaining microglia from the culture. The liposomal clodronate medium was then removed and culture plates washed before further experimentation.

Microglia activation and TUNEL staining. Microglia samples were exposed to medium containing IFNγ (R&D Systems, 285-IF; 200 ng ml^{-1}), lipopolysaccharides (LPS) (Sigma, L2654; 100 ng ml^{-1}) or a combination of both for a period of 24 h to induce an inflammatory response[32]. Cells were then processed for immunofluorescence to determine inflammation state as previously described[33]. Anti-CD11b antibody (Bio-Rad, MCA711G; 1:500) and goat anti-rat AlexaFluor 594 (Invitrogen, A-11007; 1:500) staining was counterstained with DAPI (Invitrogen, D1306; 1:1,000). To assess AP-mediated cell clearance specificity, activated or basal microglia were exposed to AP20187 (Clontech, 635059; 10 nM or 100 nM) for a period of 24 h. TUNEL staining was then performed according to the manufacturer's instructions (Roche In situ Cell Death Detection Kit, Fluorescein: 11684795910). All imaging was performed using an Olympus BX53 Fluorescence microscope and DP80 digital camera. Analysis was performed using the Fiji distribution of ImageJ (version 1.51n)[34]. To obtain a TUNEL positive percentage, a region of interest was defined using Li Auto Thresholding of the DAPI channel, and the colocalization percentage was calculated using the colocalization threshold plugin bound by that region.

IncuCyte tracking of basal and activated astrocytes. To track basal and activated astrocytic response to AP, astrocytes were plated in a 48-well culture plate (10,000 cells per well) and placed into the IncuCyte S3 Live-Cell Analysis System. The IncuCyte System is a time-lapse imaging system that records changes in cell culture through photographic capture of the culture well within the incubator. Cultures were acclimatized to the system for a period of 6 h, then exposed to medium containing IFNγ (R&D Systems, 285-IF; 200 ng ml^{-1}), LPS (Sigma, L2654; 100 ng ml^{-1}) or a combination of both for a period of 24 h to induce an inflammatory response[35]. Cells were also plated on 10-well slides and processed in tandem for immunofluorescence staining to verify activation status with anti-GFAP (DAKO, Z0334; 1:500) and counterstained with DAPI (Invitrogen, D1306; 1:1,000). After activation, astrocytes were exposed to AP20187 (Clontech, 635059; 10 nM or 100 nM) for a period of 24 h. The IncuCyte-captured phase images of each culture well were taken every 30 min over this period using the following settings: segmentation adjustment: 0.8, hole fill: 450, adjust size (pixels): −1, Minimum area (μm^2): 0.1. The phase confluency difference was calculated by subtracting the final phase confluency of each image from its initial value.

Reporting summary. Further information on research design is available in the Nature Research Reporting Summary linked to this paper.

Data availability

All source data and exact *P* values (if applicable) for every figure are included in the supporting information that accompanies the paper.

23. Kasper, L. H. et al. CREB binding protein interacts with nucleoporin-specific FG repeats that activate transcription and mediate NUP98-HOXA9 oncogenicity. *Mol. Cell. Biol.* **19**, 764–776 (1999).
24. Baker, D. J. et al. Opposing roles for $p16^{Ink4a}$ and $p19^{Arf}$ in senescence and ageing caused by BubR1 insufficiency. *Nat. Cell Biol.* **10**, 825–836 (2008).
25. Parent, J. M., von dem Bussche, N. & Lowenstein, D. H. Prolonged seizures recruit caudal subventricular zone glial progenitors into the injured hippocampus. *Hippocampus* **16**, 321–328 (2006).
26. Ly, P. T., Cai, F. & Song, W. Detection of neuritic plaques in Alzheimer's disease mouse model. *J. Vis. Exp.* **53**, 2831 (2011).
27. Oh, K. J. et al. Staging of Alzheimer's pathology in triple transgenic mice: a light and electron microscopic analysis. *Int. J. Alzheimers Dis.* **2010**, 780102 (2010).
28. Yang, Z. et al. Age-related decline in BubR1 impairs adult hippocampal neurogenesis. *Aging Cell* **16**, 598–601 (2017).
29. Kumamaru, H. et al. Liposomal clodronate selectively eliminates microglia from primary astrocyte cultures. *J. Neuroinflammation* **9**, 116 (2012).
30. Gordon, R. et al. A simple magnetic separation method for high-yield isolation of pure primary microglia. *J. Neurosci. Methods* **194**, 287–296 (2011).
31. Tsay, H. J. et al. Amyloid β peptide-mediated neurotoxicity is attenuated by the proliferating microglia more potently than by the quiescent phenotype. *J. Biomed. Sci.* **20**, 78 (2013).
32. Chao, C. C., Hu, S., Molitor, T. W., Shaskan, E. G. & Peterson, P. K. Activated microglia mediate neuronal cell injury via a nitric oxide mechanism. *J. Immunol.* **149**, 2736–2741 (1992).
33. Wang, G. et al. Apoptosis and proinflammatory cytokine responses of primary mouse microglia and astrocytes induced by human H1N1 and avian H5N1 influenza viruses. *Cell. Mol. Immunol.* **5**, 113–120 (2008).
34. Schindelin, J. et al. Fiji: an open-source platform for biological-image analysis. *Nat. Methods* **9**, 676–682 (2012).
35. Chung, I. Y. & Benveniste, E. N. Tumor necrosis factor-alpha production by astrocytes. Induction by lipopolysaccharide, IFN-gamma, and IL-1 beta. *J. Immunol.* **144**, 2999–3007 (1990).

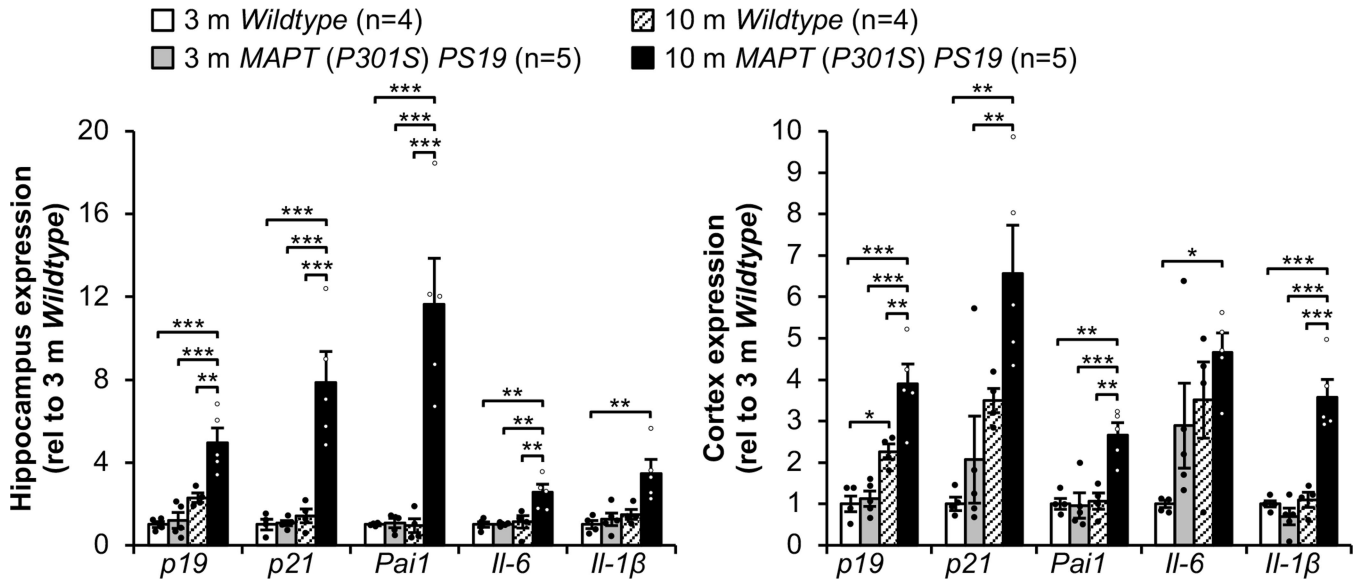

Extended Data Fig. 1 | Senescent cells accumulate in *PS19* mice. RT–qPCR analysis of senescence-associated genes in hippocampi (left) and cortices (right) of three- and ten-month-old male mice. Number of mice is as indicated, two independent experiments; normalized to the three-month wild-type group. Data are mean ± s.e.m. $*P < 0.05$; $**P < 0.01$; $***P < 0.001$ (one-way ANOVA with Tukey's multiple comparisons test). Exact *P* values can be found in the accompanying Source Data.

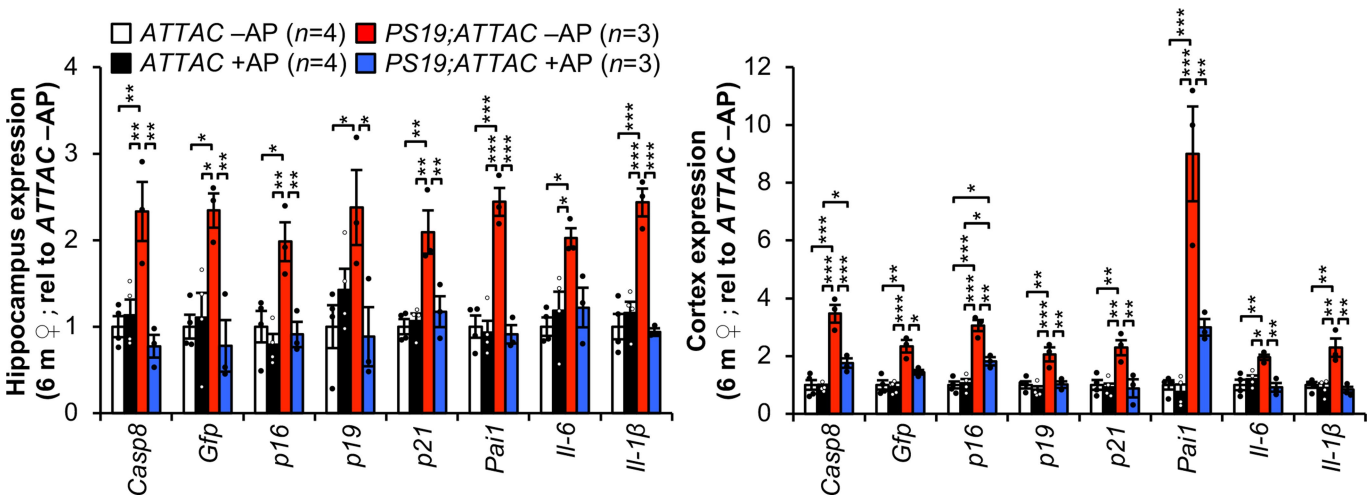

Extended Data Fig. 2 | AP-mediated clearance selectively removes senescent cells that accumulate in the brains of *PS19;ATTAC* mice. RT–qPCR analysis of the expression of senescence markers in the hippocampus (left) and cortex (right) of six-month-old female mice, treated with either vehicle (–AP) or AP20187 (+AP). Number of mice is as indicated; normalized to the *ATTAC* – AP group. Data are mean ± s.e.m. $*P < 0.05$; $**P < 0.01$; $***P < 0.001$ (one-way ANOVA with Tukey's multiple comparisons test). Exact *P* values can be found in the accompanying Source Data.

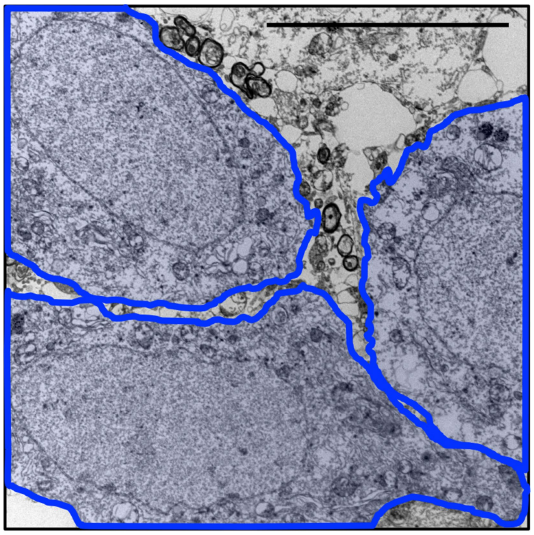

Extended Data Fig. 3 | Neurons do not exhibit X-Gal crystals upon Gal-TEM imaging. Representative electron microscopy image of neurons after SA-β-Gal staining from a six-month-old, vehicle-treated *PS19;ATTAC* male mouse ($n = 3$ male mice, 2 independent experiments). The image has been artificially coloured to show individual cell bodies. Scale bar, 10 μm.

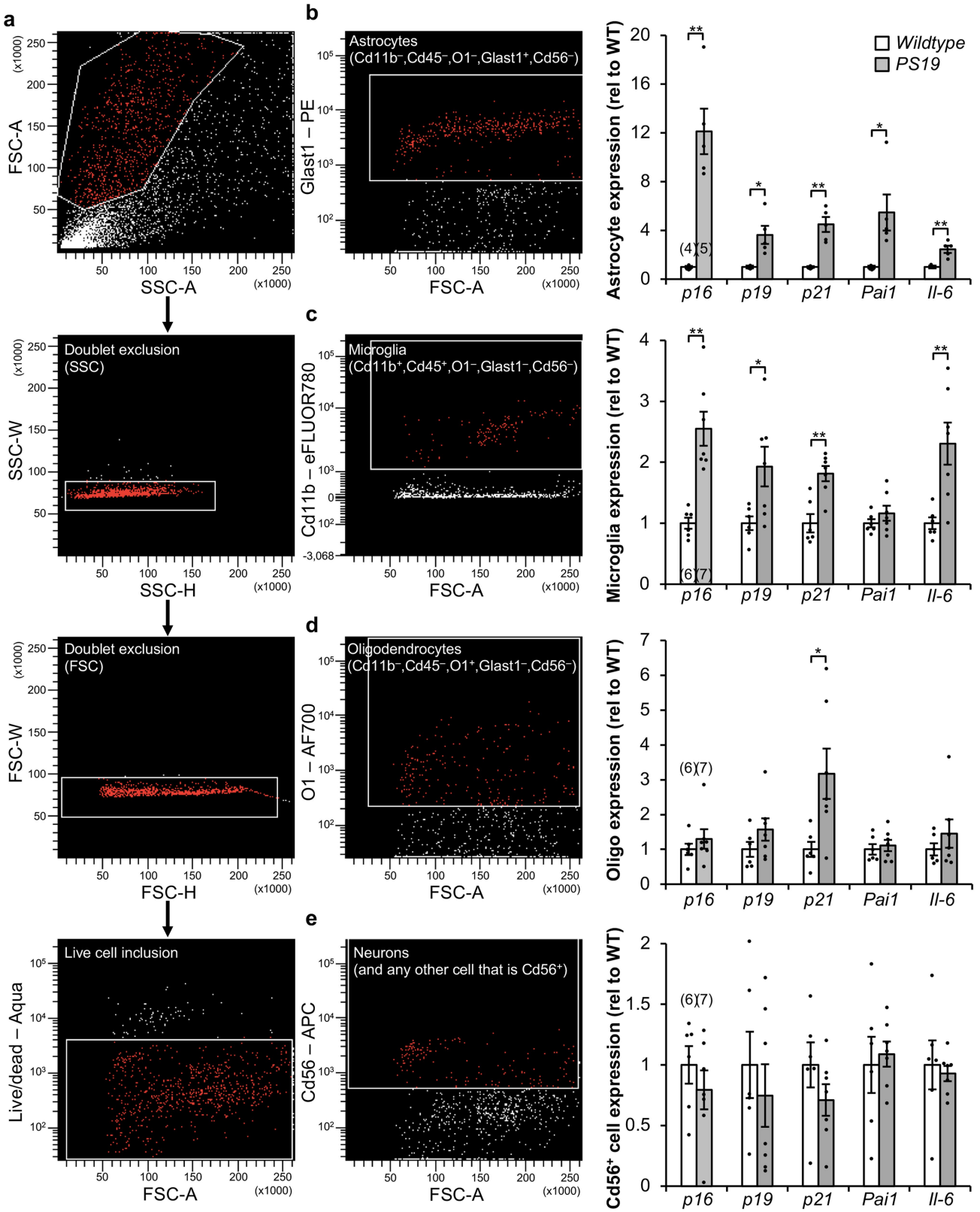

Extended Data Fig. 4 | Increased expression of senescence-associated genes is observed in astrocytes and microglia isolated from *PS19* mice. a–e, Gating strategy (**a**) for FACS isolation of living astrocytes (**b**), microglia (**c**), oligodendrocytes (**d**) and neuron-enriched CD56$^+$ cells (**e**) from cortices of six-month-old wild-type and *PS19* mice. **b**, Astrocyte (CD11b$^-$CD45$^-$O1$^-$GLAST$^+$CD56$^-$) fraction (left) and RT–qPCR analysis (right). **c**, Microglia (CD11b$^+$CD45$^+$O1GLAST$^+$CD56$^-$) fraction (left) and RT–qPCR analysis (right). **d**, Oligodendrocyte (CD11b$^-$CD45$^-$O1$^+$GLAST$^-$CD56$^-$) fraction (left) and RT–qPCR analysis (right). **e**, Neuron-enriched CD56$^+$ (CD11b$^-$CD45$^-$O1$^-$GLAST$^-$CD56$^+$) fraction (left) and RT–qPCR analysis (right). Individual numbers of independent mouse cell population isolations are indicated in the parentheses above $p16^{Ink4a}$ columns (2 independent experiments). Data are mean ± s.e.m. $^*P < 0.05$; $^{**}P < 0.01$ (unpaired two-sided *t*-tests with Welch's correction). Exact *P* values can be found in the accompanying Source Data.

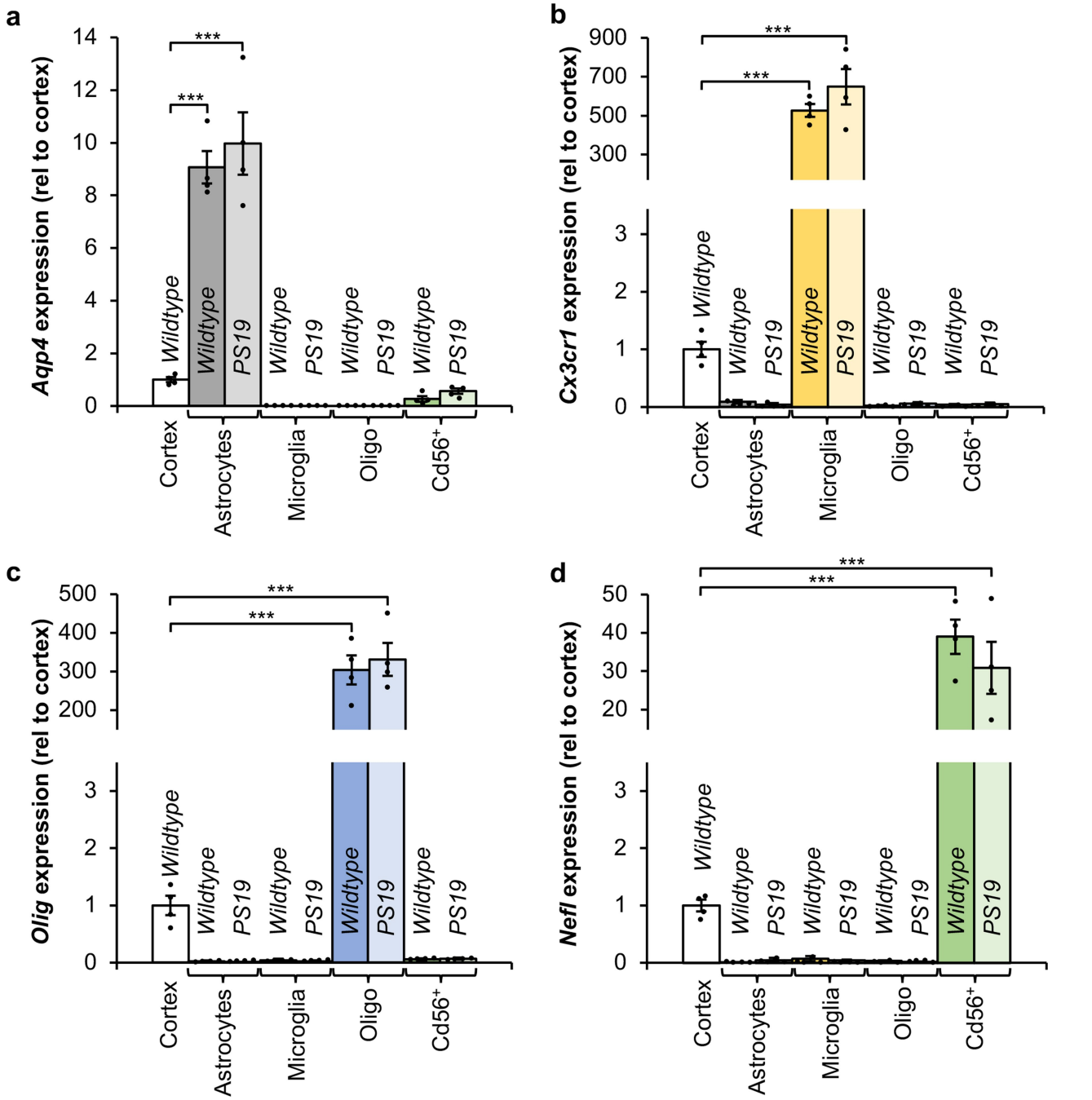

Extended Data Fig. 5 | Verification of the identity of cell populations isolated by FACS. a–d, RT–qPCR analysis of cell-identity markers from cell populations isolated from six-month-old wild-type and *PS19* mice: *Aqp4* expression enriched in astrocytes (**a**), *Cx3cr1* expression enriched in microglia (**b**), *Olig2* expression enriched in oligodendrocytes (**c**) and *Nefl* expression enriched in neurons (**d**). Expression is normalized to intact cortices of six-month-old wild-type mice ($n = 4$ biologically independent cell isolations for each group, 2 independent experiments). Data are mean ± s.e.m. ***$P < < 0.001$ (one-way ANOVA with Tukey's multiple comparisons test). Exact P values can be found in the accompanying Source Data.

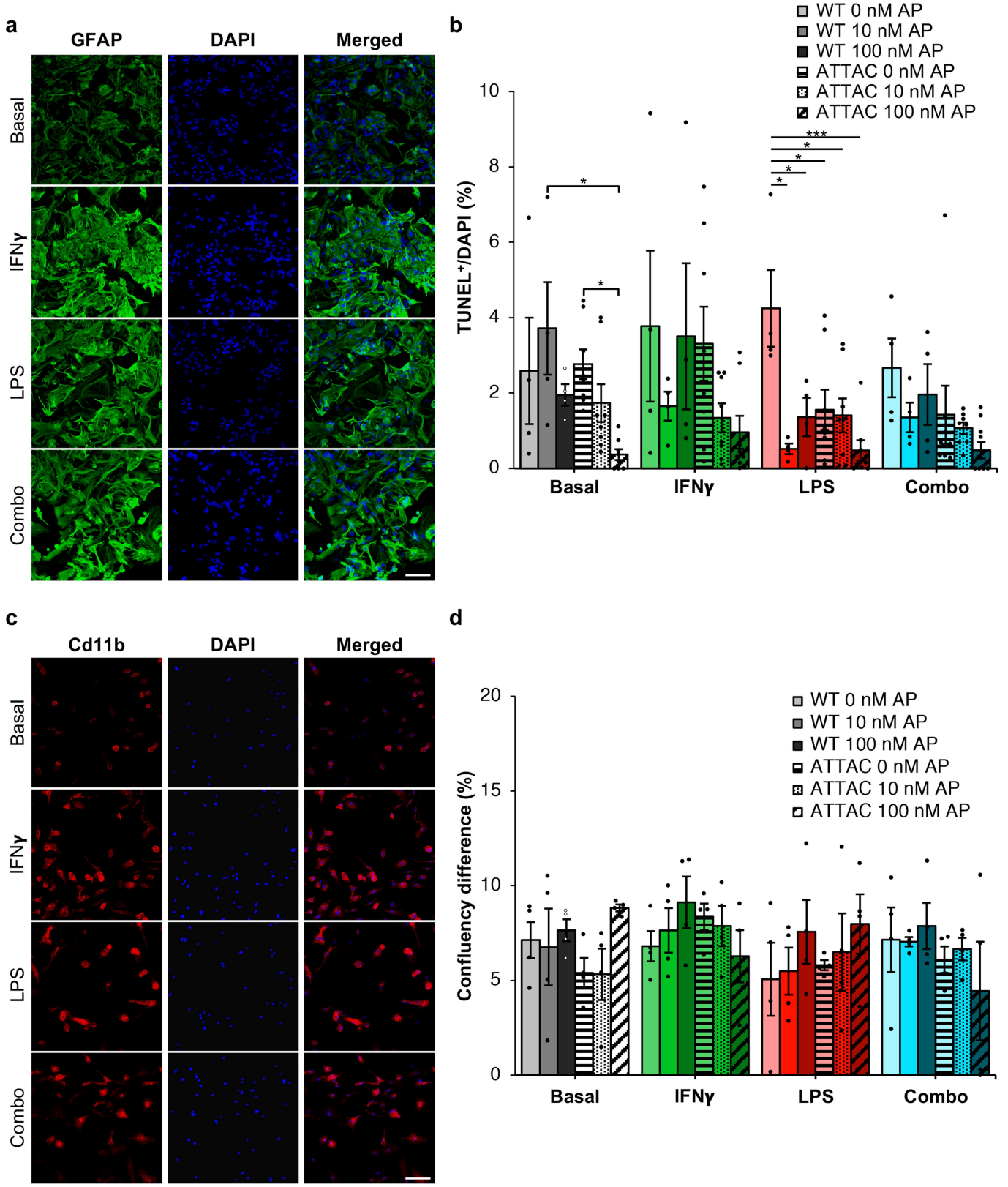

Extended Data Fig. 6 | AP administration does not erroneously eliminate non-senescent glial cells isolated from *ATTAC* mice. a, CD11b staining of primary microglia treated with IFNγ (200 ng ml^{-1}), LPS (100 ng ml^{-1}) or a combination of both ($n = 3$ biologically independent samples). **b**, Quantification of TUNEL-positive bodies in basal or activated microglia ($n = 4$ wild-type and 8 *ATTAC* cultures for each treatment group, 2 independent experiments). **c**, GFAP staining of primary astrocytes treated with IFNγ, LPS or a combination of both as described in **a** ($n = 3$ biologically independent samples). **d**, Quantification of the change in confluency over 24 h in basal or activated astrocytes ($n = 4$ biologically independent cultures of each genotype and treatment). Scale bars, 100 μm (**a**, **c**). Data are mean ± s.e.m. $^*P < 0.05$; $^{***}P < 0.001$ (one-way ANOVA with Tukey's multiple comparisons test (**b**, **d**)). Exact *P* values can be found in the accompanying Source Data.

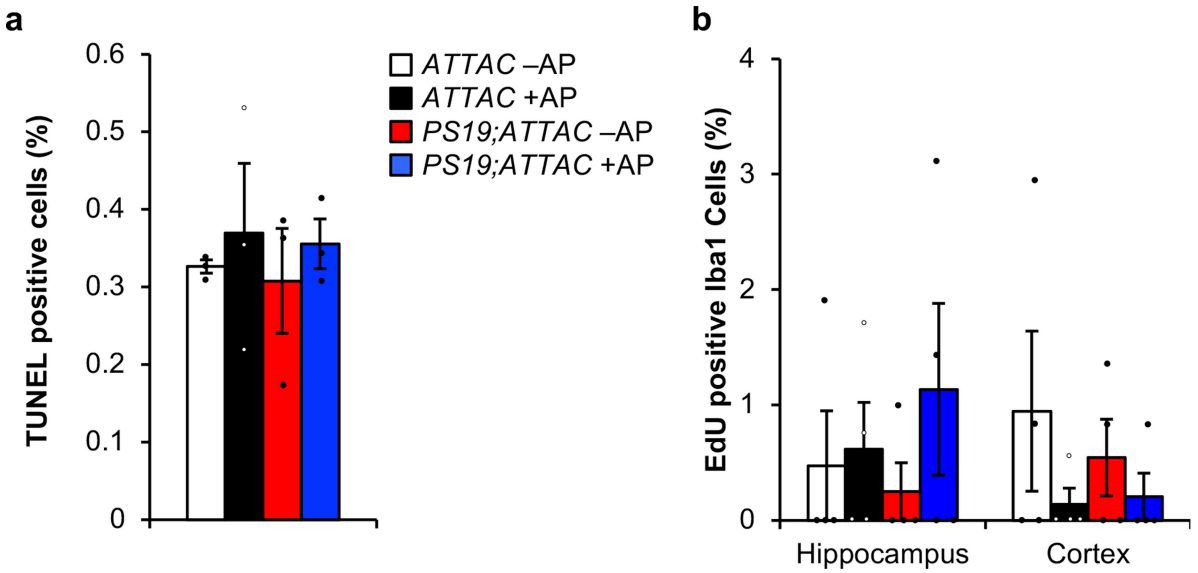

Extended Data Fig. 7 | Administration of AP does not broadly eliminate cells or increase proliferation of microglia. a, Quantification of TUNEL-positive bodies (as a percentage of all cells) at the transition between the CA2 and CA3 within the hippocampus after a short-term AP administration in six-month-old mice ($n = 3$ mice per genotype and treatment group). **b**, Quantification of IBA1/EdU double-positive cells in the hippocampus and cortex of six-month-old mice that were administered AP beginning at weaning age ($n = 4$ mice per genotype and treatment group). Data are mean ± s.e.m. We note that no comparison is statistically significant (one-way ANOVA with Tukey's multiple comparisons test). Exact *P* values can be found in the accompanying Source Data.

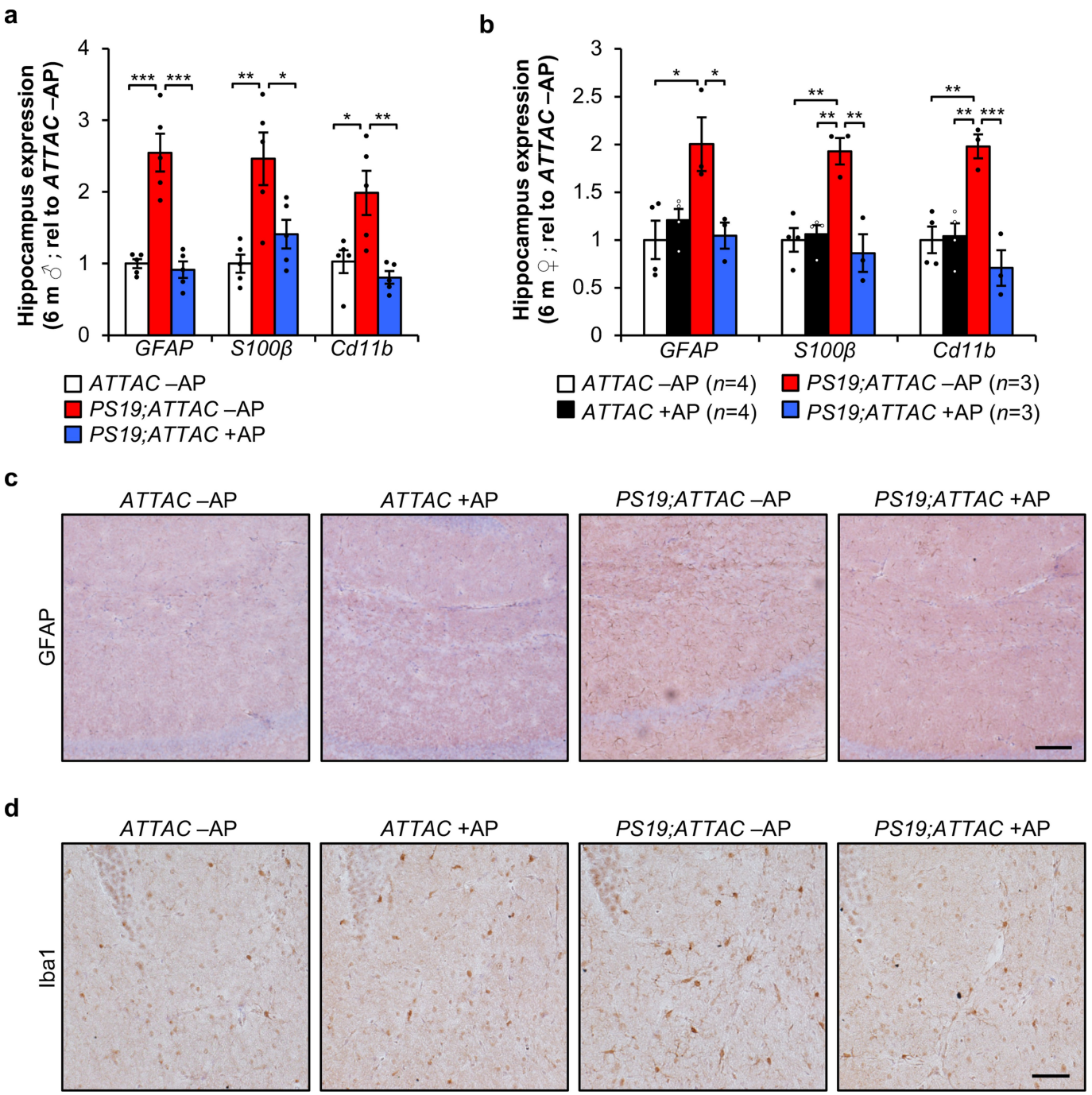

Extended Data Fig. 8 | Senescent cells promote gliosis. a, RT–qPCR analysis of *Gfap*, *S100b* and *Cd11b* in the hippocampi of six-month-old male mice ($n = 5$ mice per group; normalized to the *ATTAC* – AP group). **b**, RT–qPCR analysis as in **a** in hippocampi of six-month-old female mice (number of mice as indicated; normalized to the *ATTAC* – AP group). **c**, Representative GFAP immunohistochemistry staining in the hippocampus of six-month-old vehicle and AP-treated *ATTAC* and *PS19;ATTAC* female mice ($n = 4$ mice per group, 2 independent experiments). **d**, Representative IBA1 staining in the hippocampus of six-month-old vehicle and AP-treated *ATTAC* and *PS19;ATTAC* female mice ($n = 4$ mice per group, 2 independent experiments). Scale bar, 100 μm (**c**) and 50 μm (**d**). Data are mean ± s.e.m. $^*P < 0.05$; $^{**}P < 0.01$; $^{***}P < 0.001$ (one-way ANOVA with Tukey's multiple comparisons test). Exact *P* values can be found in the accompanying Source Data.

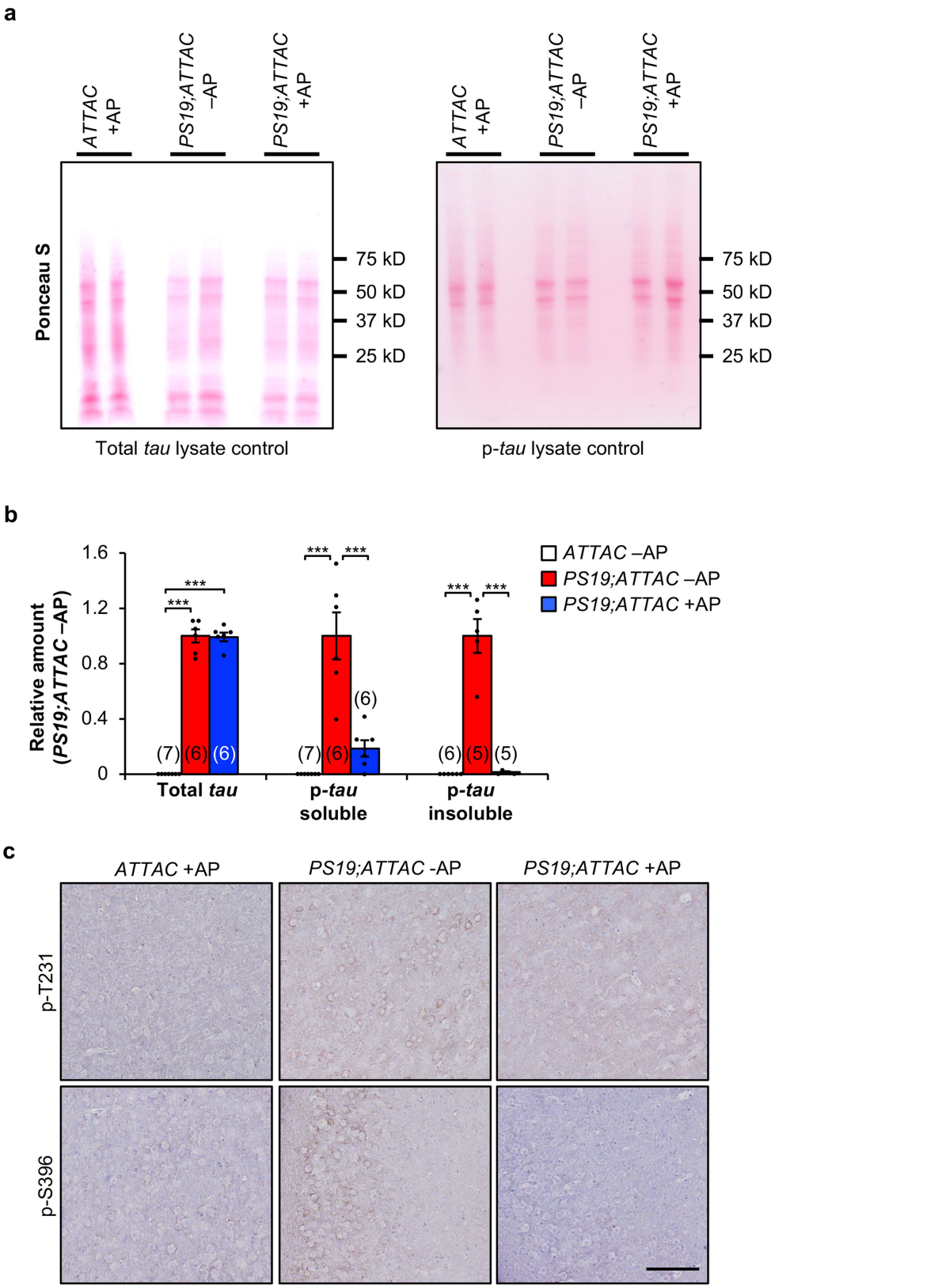

Extended Data Fig. 9 | AP treatment attenuates tau phosphorylation. **a**, Ponceau-S loading controls for the western-blot lysates of the whole brain of six-month-old mice (shown in Fig. 3a) for total tau (left) and phosphorylated tau (S202/T205; right). **b**, Quantification of the western-blot analysis of the whole brain of six-month-old mice for soluble tau (left), soluble phosphorylated tau (S202/T205; middle), and insoluble phosphorylated tau (S202/T205; right). Numbers of biologically independent mice are indicated in parentheses, data are from ≥3 independent experiments. **c**, Immunostaining of the cortex of six-month-old mice for tau protein phosphorylated at T231 (top) and S396 (bottom; $n = 4$ mice per group, 2 independent experiments). Scale bar, 100 μm. Data are mean ± s.e.m. $^{***}P < 0.001$ (one-way ANOVA with Tukey's multiple comparisons test). Exact P values can be found in the accompanying Source Data.

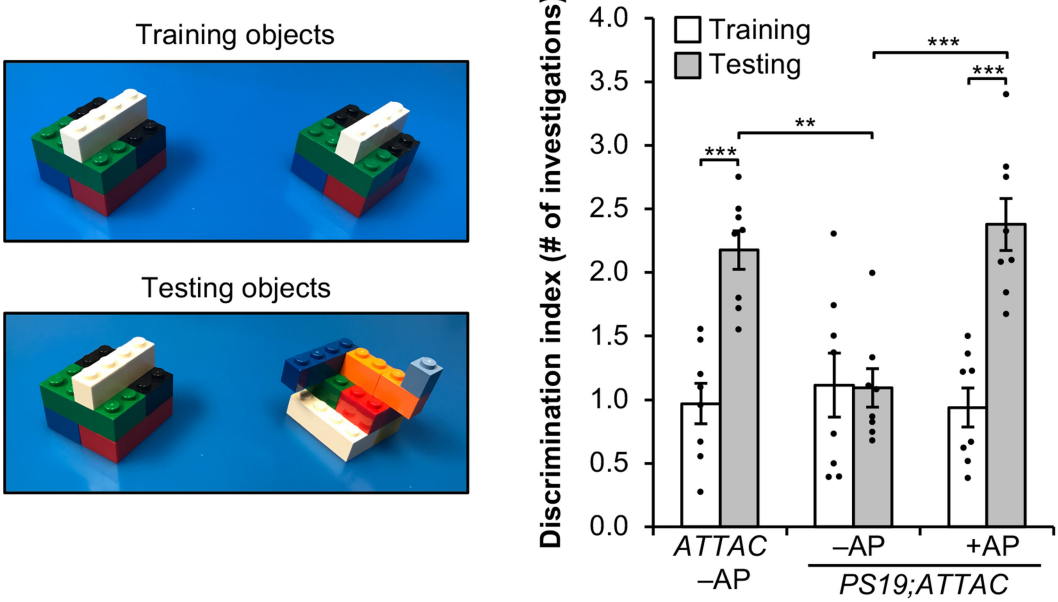

Extended Data Fig. 10 | Vision-based novel-object discrimination remains intact in AP-treated *PS19;ATTAC* mice. Objects used for novel-object recognition during the training and testing phases for visual discrimination (left) and the average ratio for the number of investigations (right, $n = 8$ female mice per group). Data are mean ± s.e.m. $^{**}P < 0.01$; $^{***}P < 0.001$ (two-way ANOVA with Tukey's multiple comparisons test). Exact P values can be found in the accompanying Source Data.

nature research

Corresponding author(s): Darren J. Baker

Reporting Summary

Nature Research wishes to improve the reproducibility of the work that we publish. This form provides structure for consistency and transparency in reporting. For further information on Nature Research policies, see Authors & Referees and the Editorial Policy Checklist.

Statistical parameters

When statistical analyses are reported, confirm that the following items are present in the relevant location (e.g. figure legend, table legend, main text, or Methods section).

n/a	Confirmed	
☐	☒	The exact sample size (*n*) for each experimental group/condition, given as a discrete number and unit of measurement
☐	☒	An indication of whether measurements were taken from distinct samples or whether the same sample was measured repeatedly
☐	☒	The statistical test(s) used AND whether they are one- or two-sided *Only common tests should be described solely by name; describe more complex techniques in the Methods section.*
☐	☒	A description of all covariates tested
☐	☒	A description of any assumptions or corrections, such as tests of normality and adjustment for multiple comparisons
☐	☒	A full description of the statistics including central tendency (e.g. means) or other basic estimates (e.g. regression coefficient) AND variation (e.g. standard deviation) or associated estimates of uncertainty (e.g. confidence intervals)
☒	☐	For null hypothesis testing, the test statistic (e.g. *F*, *t*, *r*) with confidence intervals, effect sizes, degrees of freedom and *P* value noted *Give P values as exact values whenever suitable.*
☒	☐	For Bayesian analysis, information on the choice of priors and Markov chain Monte Carlo settings
☒	☐	For hierarchical and complex designs, identification of the appropriate level for tests and full reporting of outcomes
☒	☐	Estimates of effect sizes (e.g. Cohen's *d*, Pearson's *r*), indicating how they were calculated
☐	☒	Clearly defined error bars *State explicitly what error bars represent (e.g. SD, SE, CI)*

Our web collection on statistics for biologists may be useful.

Software and code

Policy information about availability of computer code

Data collection	ImageJ was used for western blot quantification and TUNEL % calculations
Data analysis	Prism 6.0 was used for all statistical assessments.

For manuscripts utilizing custom algorithms or software that are central to the research but not yet described in published literature, software must be made available to editors/reviewers upon request. We strongly encourage code deposition in a community repository (e.g. GitHub). See the Nature Research guidelines for submitting code & software for further information.

Data

Policy information about availability of data

All manuscripts must include a data availability statement. This statement should provide the following information, where applicable:

- Accession codes, unique identifiers, or web links for publicly available datasets
- A list of figures that have associated raw data
- A description of any restrictions on data availability

All source data and exact P values (if applicable) for every figure are included in the supporting information that accompanies the paper.

Field-specific reporting

Please select the best fit for your research. If you are not sure, read the appropriate sections before making your selection.

☒ Life sciences ☐ Behavioural & social sciences ☐ Ecological, evolutionary & environmental sciences

For a reference copy of the document with all sections, see nature.com/authors/policies/ReportingSummary-flat.pdf

Life sciences study design

All studies must disclose on these points even when the disclosure is negative.

Sample size	We note that no power calculations were used. Sample sizes are based on previously published experiments where differences were observed.
Data exclusions	No samples were excluded from the analysis.
Replication	Results shown are representative of several independently performed experiments. Number of biological replicates is as described in figure legends.
Randomization	Treatment groups were randomly assigned to mice at weaning age.
Blinding	Investigators were blinded to allocation during experiments and outcomes assessment, except for rare instances where blinding was not possible.

Reporting for specific materials, systems and methods

Materials & experimental systems

n/a	Involved in the study
☐	☒ Unique biological materials
☐	☒ Antibodies
☐	☒ Eukaryotic cell lines
☒	☐ Palaeontology
☐	☒ Animals and other organisms
☒	☐ Human research participants

Methods

n/a	Involved in the study
☒	☐ ChIP-seq
☐	☒ Flow cytometry
☒	☐ MRI-based neuroimaging

Unique biological materials

Policy information about availability of materials

Obtaining unique materials	There are no restrictions.

Antibodies

Antibodies used	Western Blot - Total Tau - (ThermoFisher, MN1000; clone:n/a; lot:QC214397; 1:5000) Western Blot - Phospho-tau S202/T205 - (ThermoFisher, MN1020; clone:n/a ; lot:QJ20872020; 1:1000) IHC - Phospho-tau S202/T205 - (ThermoFisher, MN1020; clone:n/a; lot:QJ20872020; 1:500) IHC - Phospho-tau T231 - (ThermoFisher, MN1040; clone:AT180; lot:SL2484202; 1:500) IHC - Phospho-tau S396 - (Abcam, 109390; clone: n/a; lot:GR303639-17; 1:500) IHC - Gfap - (Dako, Z0334; clone:n/a; lot:20010594; 1:500) IHC - Iba1 - (Novus, NB100-1028; Lot#S7C5 E210518; Clone# n/a; 1:100) IF - NeuN - (EMD, MAB377; clone:n/a; lot:2987527; 1:200) IF - Cd11b - (BioRad, MCA711G; clone:n/a; lot:1709; 1:500) IF - Gfap - (Dako, Z0334; clone:n/a; lot:20010594; 1:500) IF - DAPI - (Invitrogen, D1306; clone:n/a; lot:1836282; 1:1000) IF - Goat anti-Rat AlexaFluor 594 - (Invitrogen, A-11007; clone:n/a; lot:1903506; 1:500) IF - Iba1 - (Wako, 019-19741; clone:n/a; lot:LKH4161; 1:500) FACS IF - LIVE/DEAD Aqua - (Invitrogen, L34966; clone:n/a; lot:1899019; 1:250) FACS IF - Cd11b eFluor 450 - (eBioscience, 48-0112-80; clone:M1/70; lot:4306306; 1:100) FACS IF - Cd45 APC eFluor 780 - (eBioscience, 47-0451-82; clone:30-F11; lot:E10101-1636; 1:200)

FACS IF - Glast1 PE - (Miltenyi Biotec, 130-095-821; clone:n/a; lot:5160331127; 1:100)
FACS IF - O1 AF 700 - (R&D Systems, FAB1327N-100UG; clone:n/a; lot:1474296; 1:100)
FACS IF - Cd56 APC (R&D Systems, FAB7820A; clone:n/a; lot:ADIK0117051; 1:100)

Validation

All antibodies are from commercially available sources and have been validated from the manufacturer with supporting publications found on manufacturer websites. See below for summary:
Western Blot - Total Tau - (ThermoFisher; MN1000)
Species: Bovine, Rat, Non-human primate, Human, Mouse
Application: ELISA, Immunocytochemistry, Immunofluorescence, Immunohistochemistry, Western Blot
Western Blot - Phospho-tau S202/T205 - (ThermoFisher, MN1020)
Species: Chicken, Dog, Fruit fly, Hamster, Human, Mouse, Non-human primate, Rabbit, Rat
Application: ELISA, Immunocytochemistry, Immunofluorescence, Immunohistochemistry, Western Blot

IHC - Phospho-tau S202/T205 - (ThermoFisher, MN1020)
Species: Chicken, Dog, Fruit fly, Hamster, Human, Mouse, Non-human primate, Rabbit, Rat
Application: ELISA, Immunocytochemistry, Immunofluorescence, Immunohistochemistry, Western Blot
IHC - Phospho-tau T231 - (ThermoFisher, MN1040)
Species: Cat, Chicken, Dog, Fruit fly, Hamster, Horse, Human, Mouse, Non-human primate, Rabbit, Rat
Application: Immunofluorescence, Immunohistochemistry, Western Blot
IHC - Phospho-tau S396 - (Abcam, 109390)
Species: Mouse, Rat, Human
Application: Dot blot, Immunohistochemistry, Western Blot
IHC - Gfap - (Dako, Z0334)
Species: Cat, Cow, Dog, Mouse, Rat, Sheep
Application: Immunohistochemistry, Immunofluorescence
IHC - Iba1 - (Novus, NB100-1028)
Species: Human, Mouse, Rat, Porcine
Application: Western Blot, Immunohistochemistry, Immunofluorescence, ELISA
IF - NeuN - (EMD, MAB377)
Species: Human, Rat, Mouse, Ferret, Chick and Salamander
Application: Immunohistochemistry, Immunofluorescence, Immunoblotting
IF - Cd11b - (BioRad, MCA711G)
Species: Mouse, Human
Application: Flow Cytometry, Immunohistology, Immunoprecipitation Immunofluorescence
IF - Gfap - (Dako, Z0334)
Species: Cat, Cow, Dog, Mouse, Rat, Sheep
Application: Immunohistochemistry, Immunofluorescence
IF - DAPI - (Invitrogen, D1306)
Species: Nucleic Acid
Application: Immunofluorescence
IF - Goat-anti-Rat AlexaFluor 594 (Invitrogen, A-11007)
Species: N/A
Application: Flow Cytometry, Immunohistochemistry, Immunofluorescence
IF - Iba1 - (Wako, 019-19741)
Species: Rat, Mouse
Application: Immunohistochemistry, Immunofluorescence, Western Blot
FACS IF - LIVE/DEAD Aqua - (Invitrogen, L34966)
Species: Eukaryotic Cells
Application: Flow Cytometry
FACS IF - Cd11b eFluor 450 - (eBioscience, 48-0112-80)
Species: Mouse, Human
Application: Flow Cytometry
FACS IF - Cd45 APC eFluor 780 - (eBioscience, 47-0451-82)
Species: Mouse, Human
Application: Flow Cytometry
FACS IF - Glast1 PE - (Miltenyi Biotec, 130-095-821)
Species: Human, Mouse, Rat
Application: Flow Cytometry, Immunofluorescence
FACS IF - O1 AF 700 - (R&D Systems, FAB1327N)
Species: Human, Mouse, Rat, Chicken
Application: Flow Cytometry
FACS IF - Cd56 APC (R&D Systems, FAB7820A)
Species: Mouse
Application: Flow Cytometry

Eukaryotic cell lines

Policy information about cell lines

Cell line source(s)	Primary astrocyte and microglia cultures generated within the laboratory from genetically modified mice.
Authentication	Antibody staining (and RT-qPCR) for cell identity was performed prior to experimentation.
Mycoplasma contamination	All cultures were primary cultures that were used at early passage. They were not tested for mycoplasm contamination.
Commonly misidentified lines (See ICLAC register)	None of the cell lines used are listed in the ICLAC database

Animals and other organisms

Policy information about studies involving animals; ARRIVE guidelines recommended for reporting animal research

Laboratory animals	P301S (MAPT) PS19 mice were purchased from The Jackson Laboratory (stock #008169) and bred to C57BL/6 for three generations. C57BL/6 ATTAC transgenic mice are as described {Baker et al., Nature 2016;Baker et al., Nature 2011}. Male PS19 mice were bred to ATTAC females to generate cohorts of ATTAC and PS19;ATTAC mice. All mice were on a pure C57BL/6 genetic background. Age range included postnatal day 1-3 for mixed glial cultures; 3, 4, 6, 8, 10, and 12 months ± 2 weeks of age for all in vivo experiments.
Wild animals	No wild animals were used in this study.
Field-collected samples	No field-collected samples were used in this study.

Flow Cytometry

Plots

Confirm that:

☒ The axis labels state the marker and fluorochrome used (e.g. CD4-FITC).

☒ The axis scales are clearly visible. Include numbers along axes only for bottom left plot of group (a 'group' is an analysis of identical markers).

☒ All plots are contour plots with outliers or pseudocolor plots.

☒ A numerical value for number of cells or percentage (with statistics) is provided.

Methodology

Sample preparation	All information is as described in the methods section.
Instrument	FACSAria IIu SORP (BD Bioscience)
Software	FACSDiva 8.0.1
Cell population abundance	The relative populations of cells were as follows (on average) from the 'live cells': Astrocytes (~27%), microglia (~14%), oligodendrocytes (~7%) and Cd56+ (~15%). Cell populations were verified with RT-qPCR for cell lineage markers.
Gating strategy	This information can be found in Extended Data Fig. 4. Additional information can be provided if necessary.

☒ Tick this box to confirm that a figure exemplifying the gating strategy is provided in the Supplementary Information.